# Supplemental Material for GS$^3$: Efficient Relighting with Triple Gaussian Splatting

ZOUBIN BI, YIXIN ZENG, CHONG ZENG, FAN PEI, XIANG FENG, KUN ZHOU, and HONGZHI WU, State Key Lab of CAD&CG, Zhejiang University, China

**ACM Reference Format:**
Zoubin Bi, Yixin Zeng, Chong Zeng, Fan Pei, Xiang Feng, Kun Zhou, and Hongzhi Wu. 2024. Supplemental Material for GS$^3$: Efficient Relighting with Triple Gaussian Splatting. In *SIGGRAPH Asia 2024 Conference Papers (SA Conference Papers '24), December 3–6, 2024, Tokyo, Japan.* ACM, New York, NY, USA, 3 pages. https://doi.org/10.1145/3680528.3687576

## 1 ABLATIONS

### 1.1 Angular Gaussian vs. MLP

In Fig. 3, we replace the appearance function with an MLP of {30, 100, 600, 100, 30}. The input of the MLP are $\boldsymbol{\omega}_i, \boldsymbol{\omega}_o$ and a 32D latent vector, and the output is a shading color. This MLP is pre-trained on 100 SGGX BRDFs with random parameters [Heitz et al. 2015]. As shown in the figure, Solely using a dedicated appearance MLP fails to model complex all-frequency appearance, unlike our representation.

### 1.2 Shadow Splatting vs. MLP

We train our representation without using the shadow splatting process (Sec. 4.2 in our paper), and directly adopt the refinement MLP alone to represent the shadow function. As shown in the figure, a pure MLP-based approach does not produce high-quality shadows as ours. Moreover, such an approach is prone to over-fitting (i.e., less generalizable than shadow splatting).

### 1.3 Shadow Refinement

We train our representation using the shadow value directly computed from splatting without the refinement MLP (Sec. 4.2 in our paper). As shown in Fig. 3, while the main features are preserved, the shadows are not as detailed as our pipeline with the refinement step.

### 1.4 MLP for Other Effects

We train our representation with the MLP for approximating other effects removed (Sec. 4.3 in our paper). In Fig. 3, we can observe noisy results where effects like interreflections should be presented. Other components in the representation tend to compensate for the effects that would have been modeled by this missing MLP, making it more prone to over-fitting.

Table 1. Ablation studies of components in our represenetation. We list the average quantitative errors in SSIM, PSNR and LPIPS of all synthetic scenes to quantify the impact of ablated components. Our choices for individual components are shown in bold.

| Ablation Variant | SSIM↑ | PSNR↑ | LPIPS↓ |
|---|---|---|---|
| **Full** | 0.9715 | 31.39 | 0.0355 |
| w/o shadow splatting | 0.9661 | 29.93 | 0.0391 |
| w/o $\Phi$ (shadow refining) | 0.9514 | 28.03 | 0.0556 |
| w/o $\Psi$ (other effects) | 0.9707 | 31.30 | 0.0366 |
| 1 basis angular Gaussians | 0.9655 | 29.70 | 0.0407 |
| 2 basis angular Gaussians | 0.9694 | 30.93 | 0.0377 |
| 4 basis angular Gaussians | 0.9709 | 31.25 | 0.0363 |
| **8 basis angular Gaussians** | 0.9715 | 31.39 | 0.0355 |
| 16 basis angular Gaussians | 0.9721 | 31.50 | 0.0350 |
| 500 images | 0.9670 | 30.61 | 0.0390 |
| 1,000 images | 0.9698 | 31.09 | 0.0370 |
| **2,000 images** | 0.9715 | 31.39 | 0.0355 |

### 1.5 Number of Basis Angular Gaussians

In Fig. 1, we evaluate the impact of the number of basis angular Gaussians on a specific scene. And Tab. 1 lists the quantitative scores averaged over all synthetic objects/scenes. Note that the qualitative differences are more obvious in the figure, compared with the differences in average scores in the table. Our current selection of 8 is made after balancing under- and over-fitting of appearance.

### 1.6 Number of Input Images

Fig. 2 evaluates the impact of input image number. And the average errors are also reported in Tab. 1. More input images improve the reconstruction quality, due to more sampling in the view/lighting domain. We observe that it requires less input images to faithfully reconstruct scenes with simple geometry and appearance (e.g., HOTDOG) than more complex ones.

## 2 METRICS

We report detailed quantitative metrics here, due to the limited space in the main paper. First, Tab. 2 lists the errors of the comparison experiments with alternative approaches that take in environment-lit input images (corresponding to Fig. 12 in the main paper). Next, Tab. 3 reports the errors of the comparisons with [Zeng et al. 2023],

Authors' address: Zoubin Bi; Yixin Zeng; Chong Zeng; Fan Pei; Xiang Feng; Kun Zhou; Hongzhi Wu, hwu@acm.org, State Key Lab of CAD&CG, Zhejiang University, 866 Yuhangtang Rd., Hangzhou, China, 310058.


*SA Conference Papers '24, December 3–6, 2024, Tokyo, Japan*

ACM ISBN 979-8-4007-1131-2/24/12
https://doi.org/10.1145/3680528.3687576

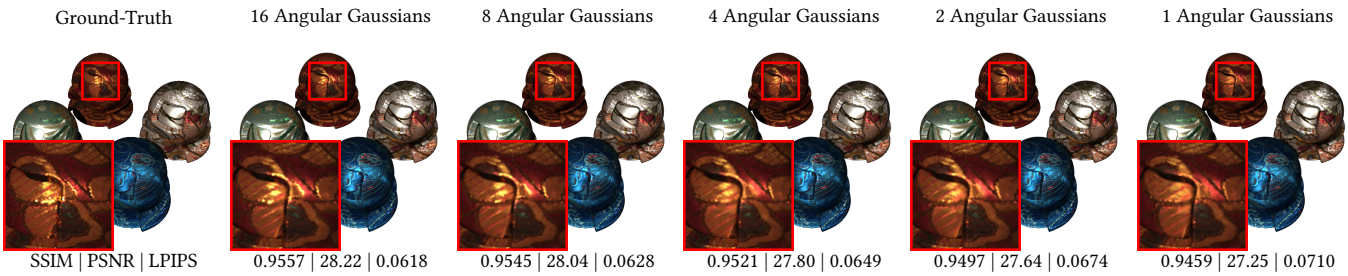


Fig. 1. Impact of the number of angular Gaussians. From the left image to right, the ground-truth, results from our representations trained with different numbers of basis angular Gaussians. Average errors in SSIM, PSNR and LPIPS are reported at the bottom of each related image.

Table 2. Quantitative metrics corresponding to Fig. 12 in the main paper. We list the quantitative errors in SSIM, PSNR and LPIPS.

| Scene | Method | SSIM↑ | PSNR↑ | LPIPS↓ |
|---|---|---|---|---|
| Hotdog | GaussianShader | 0.9439 | 29.25 | 0.0600 |
| | GS-IR | 0.9289 | 29.13 | 0.0816 |
| | Relightable3DGaussian | 0.9526 | 30.22 | 0.0555 |
| | TensoIR | 0.9590 | 31.68 | 0.0466 |
| | Ours | **0.9712** | **36.47** | **0.0342** |
| Lego | GaussianShader | 0.8964 | 24.33 | 0.0834 |
| | GS-IR | 0.9230 | 27.66 | 0.0550 |
| | Relightable3DGaussian | 0.9463 | 30.31 | 0.0446 |
| | TensoIR | 0.9540 | 30.96 | 0.0356 |
| | Ours | **0.9651** | **32.06** | **0.0302** |
| MaterialBalls | GaussianShader | 0.8900 | 24.31 | 0.0937 |
| | GS-IR | 0.8756 | 23.41 | 0.0969 |
| | Relightable3DGaussian | 0.9045 | 25.34 | 0.0848 |
| | TensoIR | 0.9026 | 25.05 | 0.0765 |
| | Ours | **0.9459** | **28.01** | **0.0508** |

Table 3. Per-object/scene quantitative comparison with NRHints [Zeng et al. 2023] (corresponding to Fig. 9 in the main paper). We list the quantitative errors in SSIM, PSNR and LPIPS.

| Scene | Method | SSIM↑ | PSNR↑ | LPIPS↓ |
|---|---|---|---|---|
| Drums | NRHints | **0.9745** | 29.88 | 0.0294 |
| | Ours | 0.9714 | **30.45** | **0.0276** |
| FurBall | NRHints | 0.9522 | 35.06 | 0.0777 |
| | Ours | **0.9669** | **35.34** | **0.0534** |
| Lego | NRHints | **0.9583** | 29.90 | **0.0393** |
| | Ours | 0.9511 | **30.19** | 0.0468 |
| Fish | NRHints | 0.9140 | **31.28** | 0.1137 |
| | Ours | **0.9252** | 31.13 | **0.0866** |
| Cluttered | NRHints | 0.9280 | 29.61 | 0.0879 |
| | Ours | **0.9521** | **30.82** | **0.0696** |
| Cat | NRHints | 0.8560 | **27.34** | 0.1667 |
| | Ours | **0.8981** | 26.43 | **0.1381** |

Table 4. Per-object/scene quantitative errors of our approach for all synthetic and captured examples.

| Scence | SSIM | PSNR | LPIPS |
|---|---|---|---|
| AnisoMetal | 0.9494 | 27.25 | 0.0462 |
| Drums | 0.9714 | 30.45 | 0.0276 |
| FurBall | 0.9669 | 35.34 | 0.0534 |
| Hotdog | 0.9733 | 32.98 | 0.0295 |
| Lego | 0.9511 | 30.19 | 0.0468 |
| Translucent | 0.9740 | 32.34 | 0.0318 |
| Cup | 0.9905 | 32.74 | 0.0203 |
| Egg | 0.9833 | 31.84 | 0.0257 |
| Fabric | 0.9812 | 31.15 | 0.0317 |
| MaterialBalls | 0.9545 | 28.04 | 0.0628 |
| Tower | 0.9913 | 32.96 | 0.0150 |
| Boot | 0.8980 | 28.84 | 0.1013 |
| Container | 0.9745 | 36.65 | 0.016 |
| Fox | 0.9225 | 34.21 | 0.0745 |
| Li'lOnes | 0.9809 | 38.61 | 0.0182 |
| Nefertiti | 0.956 | 36.58 | 0.0434 |
| Zhaojun | 0.9321 | 32.08 | 0.1071 |

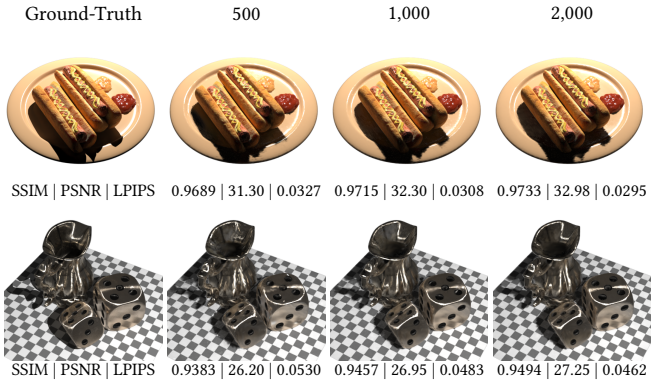


Fig. 2. Impact of the number of training images. From the left column to right, the ground-truths, and reconstruction results trained with 500, 1,000 and 2,000 images. Average errors in SSIM, PSNR and LPIPS are reported at the bottom of each related image.

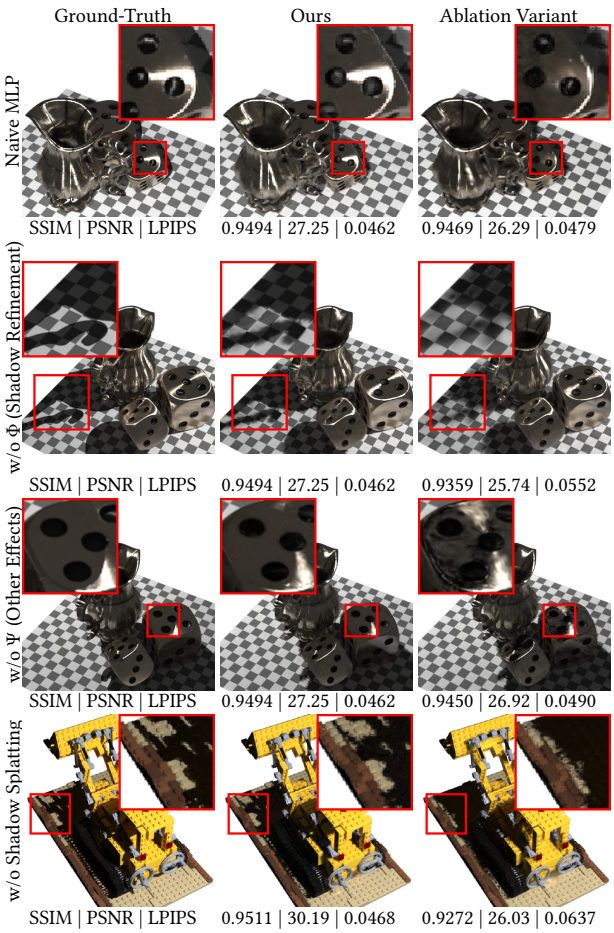


Fig. 3. Ablation studies on components of our pipeline. From the left column to right, the ground-truth, our results and results from the variants. From the top row to bottom, solely using an MLP as appearance function, removing shadow refinement step, removing the modeling of other effects, and removing shadow splatting and directly resorting to an MLP. Average errors in SSIM, PSNR and LPIPS are reported at the bottom of each related image.

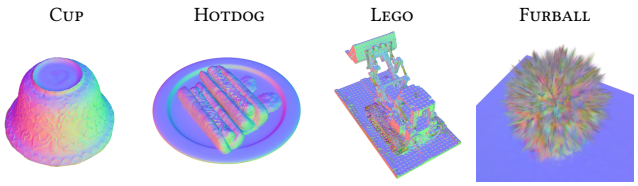


Fig. 4. Visualization of the normals of spatial Gaussians in additional scenes. Each spatial Gaussian is splatted with the pseudo color of its normal.

the best-quality method that takes in point-lit input images (corresponding to Fig. 9 in the main paper). Finally, Tab. 4 shows the errors for each synthetic and captured object/scene in this paper (corresponding to Fig. 5 and 11 in the main paper). Please refer to Sec. 5 for more details about the objects/scenes.

## 3 VISUALIZATION

In addition to Fig. 8 of the main paper, here we visualize of the normals of spatial Gaussians for additional scenes in Fig. 4.

## REFERENCES

Eric Heitz, Jonathan Dupuy, Cyril Crassin, and Carsten Dachsbacher. 2015. The SGGX microflake distribution. *ACM Transactions on Graphics (TOG)* 34, 4 (2015), 1–11.

Chong Zeng, Guojun Chen, Yue Dong, Pieter Peers, Hongzhi Wu, and Xin Tong. 2023. Relighting Neural Radiance Fields with Shadow and Highlight Hints. In *ACM SIGGRAPH 2023 Conference Proceedings*.